



Thermodynamics of slush and snow–ice formation in the Antarctic sea-ice zone

Mathilde Jutras, Martin Vancoppenolle, Antonio Lourenço, Frédéric Vivier, Gauthier Carnat, Gurvan Madec, clement rousset, Jean-Louis Tison

► To cite this version:

Mathilde Jutras, Martin Vancoppenolle, Antonio Lourenço, Frédéric Vivier, Gauthier Carnat, et al.. Thermodynamics of slush and snow–ice formation in the Antarctic sea-ice zone. Deep Sea Research Part II: Topical Studies in Oceanography, 2016, 131, pp.75-83. 10.1016/j.dsr2.2016.03.008 . hal-01303755

HAL Id: hal-01303755

<https://hal.sorbonne-universite.fr/hal-01303755>

Submitted on 18 Apr 2016

HAL is a multi-disciplinary open access archive for the deposit and dissemination of scientific research documents, whether they are published or not. The documents may come from teaching and research institutions in France or abroad, or from public or private research centers.

L'archive ouverte pluridisciplinaire **HAL**, est destinée au dépôt et à la diffusion de documents scientifiques de niveau recherche, publiés ou non, émanant des établissements d'enseignement et de recherche français ou étrangers, des laboratoires publics ou privés.

Thermodynamics of slush and snow-ice formation in the Antarctic sea-ice zone

Mathilde Jutras^{a,b}, Martin Vancoppenolle^a, Antonio Lourenço^a, Frédéric Vivier^a,
Gauthier Carnat^c, Gurvan Madec^a, Clément Rousset^a, Jean-Louis Tison^c

^a*LOCEAN-IPSL, Sorbonne Universités (UPMC Paris 6), CNRS/IRD/MNHN, Paris, France.*

^b*Department of Atmospheric and Oceanic Sciences, McGill University, Montreal, Quebec, Canada.*

^c*Laboratoire de Glaciologie, Université Libre de Bruxelles, Belgium.*

Abstract

Snow over Antarctic sea ice is often flooded by brine or seawater, particularly in spring, forming slush and snow ice. Here, we evaluate the representation of the thermodynamics of slush and snow-ice formation in large-scale sea-ice models, using laboratory experiments (NaCl solutions poured into grated ice in an isolated container). Scaling analysis highlights latent heat as the main term of the energy budget. The temperature of the new sea ice immediately after flooding is found very close to the saltwater freezing point, whereas its bulk salinity is typically > 20 g/kg. Large-scale sea-ice models faithfully represent such physics, yet the uncertainty on the origin of flooding saltwater impacts the calculated new ice temperature, because of the different salinities of seawater and brine. The laboratory experiments also suggest a potential limitation to the existing physical representations of flooding: for brine fractions $> 60\%$, ice crystals start floating upon saltwater. Natural sea-ice observations suggest that the isolated system assumption holds for a few hours at most, after which rapid heat and salt exchanges mostly destroy the initial flooding signature on temperature and salinity. A small footprint on ice salinity remains however: natural snow ice is found 3-5 g/kg more saline than other forms of sea ice.

9 *Keywords:* snow ice, Antarctic, slush, thermodynamics

10 **1. Introduction**

11 The Antarctic sea-ice environment is highly dynamic, characterized by the fre-
 12 quent passage of storms (Worby et al., 1998), the influence of ocean waves (Squire,
 13 2007) and substantial precipitation (Bromwich et al., 2004). Such conditions force
 14 the redistribution and mixing of pure ice, snow, seawater, brine and meltwa-
 15 ter within the pack, as indicated by the diverse texture and isotopic signals in
 16 Antarctic compared to Arctic sea ice (Jeffries et al., 1997). The processes mixing
 17 ice, snow and water are mainly the flooding of snow by seawater and brine (e.g.
 18 Lytle and Ackley, 1996), the percolation of meltwater through the brine network
 19 with possible stagnation and refreezing within the ice (e.g. Kawamura et al., 1997),
 20 and ice ridging, which traps seawater among broken ice blocks (e.g. Leppäranta et al.,
 21 1995; Tin and Jeffries, 2003; Williams et al., 2014). In turn, the main Antarc-
 22 tic sea ice halo-thermodynamic regimes (Haas et al., 2001; Kawamura et al., 1997;
 23 Maksym and Jeffries, 2000; Saenz and Arrigo, 2012) are more diverse than the stan-
 24 dard Arctic modeling view suggests (e.g. Maykut and Untersteiner, 1971).

25 In particular, flooding of the snow base is widespread in the Antarctic sea-
 26 ice zone, fostered by two specificities: relatively small ice thickness (Worby et al.,
 27 2008) and abundant snowfall, often exceeding 500 mm of water equivalent per year
 28 (Bromwich et al., 2004; Jeffries et al., 2001). As a result, the snow-ice interface
 29 is often pushed below sea level (negative freeboard), hydraulically forcing the in-
 30 filtration of saltwater into snow, forming slush and snow ice (Eicken et al., 1994;
 31 Lytle and Ackley, 1996). The flooding water can be brine moving upwards, if the
 32 ice is permeable (Golden et al., 1998), or seawater moving laterally from cracks and
 33 floe edges (Massom et al., 2001). The snow-ice thickness is highest in late winter

in coastal regions of the East Antarctic sector and of the Amundsen and Belling-
 shausen Seas (Maksym and Markus, 2008). In the Northern Hemisphere, there
 are much fewer reports of slush and snow ice, because of generally thicker ice and
 much lower precipitation, as confirmed in large-scale model sea ice hindcasts (e.g.,
 Vancoppenolle et al., 2009). Yet snow ice has been reported near the coast of Sval-
 bard (Høyland, 2009) and in the Baltic Sea (Leppäranta, 1983). Slush and snow
 ice contribute to about a third of the total Antarctic sea-ice mass production, as
 suggested by oxygen isotope analyses (Jeffries et al., 1997; Worby et al., 1998), satel-
 lite (Maksym and Markus, 2008) and model-based (Vancoppenolle et al., 2009) esti-
 mates.

Slush and snow-ice formation has long been represented in large-scale sea-ice
 models as a single process (e.g., Fichefet and Morales Maqueda, 1997; Hunke et al.,
 2015; Vancoppenolle et al., 2009). The rate of snow-ice growth is determined by the
 fraction of snow depth lying below sea level, as determined by isostasy (Leppäranta,
 1983). The initial temperature and salinity of the newly formed slush / snow ice
 derive from salt and energy conservation as proposed by Schmidt et al. (2004). This
 model representation of snow-ice thermodynamics has not been evaluated with ob-
 servations, however. Process studies with one-dimensional models have focused on
 the rate of snow-ice formation (e.g. Crocker and Wadhams, 1989; Leppäranta, 1983),
 on the impact of the brine flow on the salinity evolution (Maksym and Jeffries, 2000,
 2001; Saenz and Arrigo, 2012), whereas Saenz and Arrigo (2012) also treat the im-
 pact of slush desalination on the growth of ice algae. Yet the energetic aspects of
 flooding events and their impact on the initial slush and snow-ice thermodynamic
 properties, have not been investigated. In this context, the present study aims (i) to
 describe the energy and salt budget of slush and snow-ice formation; and (ii) to eval-
 uate the thermodynamic computation of initial slush and snow-ice properties from

60 large-scale sea-ice models, using laboratory experiments.

61 We first describe (Section 2) two approaches for the energy budget of slush and
 62 snow-ice formation. The first one simplifies the energy budget but is not fully energy-
 63 conserving. The second one is based on energy and salt conservation (Schmidt et al.,
 64 2004) and used in large-scale sea ice models. The realism of both approaches is
 65 investigated through laboratory experiments. In these experiments, described in
 66 Section 3, a NaCl solution is poured within grated ice (a lab analog for snow) in
 67 a cryogenic container, varying the physical input conditions (the temperature of
 68 both snow and saltwater, the saltwater salinity, and the grated ice density). Both
 69 theoretical approaches suggest that the temperature of the initial slush is very close
 70 to the freezing point of the flooding saltwater, which is confirmed experimentally
 71 (Section 4). Yet we find a significant limit in the validity of both representations
 72 of the process: if the liquid fraction exceeds 60%, the ice crystals start to float,
 73 stratifying the system into two layers with distinct properties. In Section 5, results
 74 are put in the context of natural sea-ice observations. In Section 6, we provide
 75 elements of discussion and conclude this paper.

76 2. Theoretical Background

77 As assumed in large-scale sea-ice models, freshly formed slush and snow ice
 78 are not explicitly distinguished: both are considered as sea ice, characterized by
 79 temperature (T , in $^{\circ}\text{C}$) and bulk salinity (S , in g/kg) (Bitz and Lipscomb, 1999;
 80 Vancoppenolle et al., 2010). Hence, and unless otherwise stated, we will hereafter
 81 use *snow ice* both for *slush* and *snow ice*. The transformation of a mixture of snow
 82 and saltwater into sea ice is considered (see illustrations of the process as occurring
 83 in the field in Fig. 1a and as conceptualized in Fig. 1b). The initial state of the
 84 system is characterized by a snow mass m_s , with temperature T_s , zero salinity, and

density ρ_s , homogeneously flooded by saltwater with mass m_w , temperature T_w and salinity S_w . The final state is a mass of sea ice m_i with temperature T_i , salinity S_i and density ρ_i . Note that we neither consider the neighbouring dry snow above or sea ice below (see Fig. 1a), nor the pathway, nor the origin of the flooding water.

2.1. The freezing-point approach

The first approach to derive the snow-ice temperature shortly after formation is based on physical reasoning. For the snow temperatures $[-10^\circ\text{C}, 0^\circ\text{C}]$ and saltwater temperatures $[-2^\circ\text{C}, 2^\circ\text{C}]$ encountered in nature, the Stefan number cT/L is generally small (< 0.05). Therefore, the sensible heat stored in saltwater and snow is generally much smaller than the latent heat released (absorbed) due to internal freezing (melting). Hence, only a small amount of internal freezing (melting) is required to compensate for the sensible heat of the two initial phases. Because of the small internal melting or freezing, the salinity of the brine incorporated in new snow ice is close to the flooding saltwater salinity S_w . Assuming thermal equilibrium and linear liquidus, one finds that the temperature of the new snow ice is simply:

$$T \approx T^{fr} = -\mu S_w, \quad (1)$$

where μ gives the linear dependence of the freezing temperature as a function of water salinity and differs for seawater and NaCl solutions (see Tab. 1). In this view, the new snow-ice temperature is the freezing point of the flooding saltwater T^{fr} . Whereas this *freezing point approach* seems suitable for a physical description of the process, it may not be valid in all conditions. In addition, because sensible heat is neglected, the freezing point approach is not energy-conserving, and hence not appropriate for large-scale models.

2.2. The fully energy- and salt-conserving approach

In most sea-ice models, the temperature and salinity of solid and liquid mixtures right after formation derive from mass, salt and energy conservation equations (Schmidt et al., 2004). Following this generic approach, hereafter referred to as *fully-conserving*, the enthalpy of snow ice is computed as the sum of the enthalpies of snow and flooding saltwater (Hunke et al., 2015; Vancoppenolle et al., 2009). From enthalpy, the ice temperature can be retrieved. The new snow-ice salinity (on which enthalpy also depends) derives from the original salt content of saltwater. This computation is shortly described in this Section. Details are given in Appendix A.

In models, flooding is typically conditioned by negative freeboard, following Leppäranta (1983), generally assuming that seawater floods the snow (Fichefet and Morales Maqueda, 1997; Hunke et al., 2015; Vancoppenolle et al., 2009), whereas in reality both brine and seawater contribute, depending on environmental conditions (Maksym and Jeffries, 2000; Massom et al., 2001). As the salinity of the flooding saltwater is treated as an independent variable, the fully-conserving approach encompasses both cases.

The following working hypotheses are made.

H1: The system is isolated, i.e. mass, salt and energy are conserved. Note that in sea-ice models, this hypothesis is only used to compute initial T and S , and relieved elsewhere, enabling external exchanges of heat and salt.

H2: The system is homogeneous and in thermodynamic equilibrium by the end of the transformation, with single values for T_i and S_i .

H3: The flooding water entirely fills the air interstices initially present in the snow.

The two relevant equations for salt and energy conservation are (see Appendix A

for a complete derivation):

$$S_i = \phi_a S_w \quad (2a)$$

$$E_i(T_i, S_i) = \phi_i E_s(T_s) + \phi_a E_w(T_w) \quad (2b)$$

where $\phi_i = \rho_s/\rho_i$ and $\phi_a = (\rho_i - \rho_s)/\rho_i$ are respectively the ice and air fractions in the pre-existing snow, and E_i , E_s and E_w are the specific enthalpies (in J/kg) of sea ice, snow and saltwater, respectively (Schmidt et al., 2004). The system of equations (2) thermodynamically describes new sea-ice formation due to flooding, giving S_i and T_i , as a function of T_w , S_w , T_s and ρ_s . The enthalpy-temperature diagram (Fig. 2) graphically illustrates the links between the energy budget and temperature. In agreement with the physical scaling of Section 2.1, the E-T diagram indicates that the latent heat dominates the energy budget. In the rare case snow density would exceed $\approx 2/3\rho_i \approx 600 \text{ kg/m}^3$, sensible heat storage in snow would significantly contribute to the energy budget as well.

Snow density over Antarctic sea ice features large variations in the 100-600 kg/m^3 range, with typical values around 320-360 kg/m^3 (Massom et al., 2001). Deep snow is generally denser. Since the value $\rho_s = 330 \text{ kg/m}^3$ introduced by Maykut and Untersteiner (1971) is still a standard value in present-day sea ice models (Bitz and Lipscomb, 1999; Vancoppenolle et al., 2009), we used it here as a basis for theoretical computations (e.g. Fig. 2 and 3). The chosen value of 950 kg/m^3 for sea ice density corresponds to $\sim 35\%$ of brine fraction, substantially higher than pure ice density (917 kg/m^3).

The salinity equation is trivial, whereas the enthalpy equation can be rewritten as a second-order algebraic equation for sea-ice temperature, with a unique physically-

157 acceptable solution:

$$158 \quad 0 = c_0 T_i^2 - A(T_w, S_w, T_s) \cdot T_i - \phi_a L \mu S_w, \quad (3)$$

$$159 \quad A(T_w, S_w, T_s) = \phi_i c_0 T_s + \phi_a \left[L + c_w T_w + (c_w - c_0) \mu S_w \right].$$

160

161 Eq. 3 gives the fully-conserving solution T^{cons} for the new snow-ice temperature.
 162 The dependence of T^{cons} on all four parameters is illustrated with the black lines in
 163 Figure 3.

164 A first-order, analytically useful solution that reasonably approximates T^{cons} can
 165 be derived by dropping the quadratic and the $(c_w - c_0) \mu S_w$ terms in the temperature
 166 equation:

$$167 \quad T_i \approx -\mu S_w \left[1 - \rho_s / (\rho_i - \rho_s) \cdot \frac{c_0 T_s}{L} - \frac{c_w T_w}{L} \right] \quad (4)$$

168 If the Stefan number (cT/L) is small, eq. 4 further reduces to $T_i \approx -\mu S_w$, i.e. the
 169 freezing point solution.

170 3. Laboratory Experiments

171 The idealized view of snow-ice formation described in Section 2 was experimen-
 172 tally emulated by enforcing the physical hypotheses **H1-H3**, using the following
 173 experimental design :

- 174 1. Place grated ice with known volume, mass (hence density) and temperature in
 175 an insulated cryogenic container.
- 176 2. Pour saltwater of known temperature and salinity until all grated ice crystals
 177 are visibly in contact with water.
- 178 3. Let the system equilibrate.
- 179 4. Measure the resulting saltwater ice properties (temperature and salinity).

180 The experimental setup is schematically illustrated in Figure 1c.

181 Grated ice, as snow, is made up of air and small ice chunks, and used here as an
 182 easily produced lab analog for snow. The structure of grated ice and of synthetic
 183 snow ice was examined in a cold room, photographed and compared to natural snow
 184 ice from the SIMBA campaign (Lewis et al., 2011), see Figure 4. Grated ice grains
 185 are larger and more acute than for natural snow (Fig. 4a), which has a visible impact
 186 on the resulting synthetic snow-ice structure (Fig. 4b-c) as compared with natural
 187 snow ice (Fig. 4d). Despite these differences, grated ice with a grain size < 2 mm
 188 is, as far as heat diffusion is concerned, comparable to snow at the scale of our
 189 experiment (10 cm).

190 The experiment was repeated at various grated ice and water temperatures (from
 191 -26.3°C to -0.8°C and from -1.2°C to 23.7°C , respectively), grated ice densities
 192 (from 332 kg/m^3 to 582 kg/m^3) and water salinities (from 22 g/kg to 69 g/kg), see
 193 Table S1. Although some of these salinity and temperature values may seem off the
 194 observed range, they enable a complete experimental check of the two models over a
 195 wide range of situations. In particular, grated ice density is larger than typical snow
 196 values (max. $\sim 390\text{ kg/m}^3$ according to Massom et al. (2001)). Grated ice is hard
 197 to control experimentally (see Appendix B), however.

198 This setup fulfills our hypotheses. **H1** (isolated system) was achieved by using
 199 a highly isolated cryogenic container (KGW-Isotherm) and by correcting the tem-
 200 perature increase due to a small heat input over the time of the experiment. The
 201 mean correction is 0.63°C for a 20 minute experiment, as retrieved from control runs
 202 measuring how water temperature increases over long periods. **H2** (homogeneous
 203 system at equilibrium) was achieved by delicately mixing to avoid stratification and
 204 interference with ice growth until the temperature stabilized. The experiments with
 205 presumed stratification were removed from the analysis (see next section). **H3** (ap-

206 appropriate water volume) was enforced by pouring water until all grated ice interstices
 207 were filled with saltwater. More details on the experimental setup, T and S measure-
 208 ments techniques and precisions are provided in Appendix B.

209 4. Results

210 We now analyze the equilibrium ice temperature, salinity and brine fraction from
 211 theory (Section 2) and experimental results. The ice salinity is trivially determined
 212 from saltwater salinity and snow density (eq. 2a). In the lab, the ice salinity is
 213 practically constrained by the amount of saltwater poured into the container. Figure
 214 5 shows the experimental snow-ice temperature versus the fully-conserving compu-
 215 tation (eq. 3). Figure 6 shows how the experimental snow-ice temperature depends
 216 on water salinity, water temperature and snow temperature. All the experimental
 217 results (T_w , T_s , ρ_s , S_w , T_i) are given in Supplementary Table S1.

218 4.1. Temperature

219 In all of our experiments, snow is initially colder than water, as is most frequently
 220 the case in nature. Therefore, once both phases are mixed, the ice grains gain heat,
 221 whereas saltwater loses heat and some water molecules freeze on existing ice crystals.
 222 This releases latent heat and increases the salinity of the remaining saltwater. The
 223 thermistors, initially lying in the ice crystals, typically record a rapid temperature
 224 increase. Temperature stabilizes within 20 minutes. Salt diffuses much more slowly
 225 than heat and sets this time scale towards equilibrium ($t \approx L^2/D \approx 20$ min, with
 226 $D = 10^{-9}$ m²/s the molecular diffusivity of salt and $L \approx 1$ mm for grated ice grains,
 227 see Fig. 4).

228 The temperatures retrieved from the fully-conserving approach (T^{cons} , eq. 3),
 229 using the experimental values of T_s , T_w , ρ_s , S_w as input parameters, closely match

the experimental equilibrium temperatures (Fig. 5 and Tab. S1), with low bias (0.07°C) and root mean square error (RMSE) ($0.19 \pm 0.22^\circ\text{C}$). The freezing point temperatures T^{fr} , based on S_w alone, are slightly less precise, with a negative bias of -0.28°C and larger RMSE ($0.36 \pm 0.48^\circ\text{C}$). Despite the small differences between T^{fr} and T^{cons} , their value is very close for a wide range of input physical parameters (see Fig. 3, dotted lines vs full lines). Indeed, when linearly regressing the retrieved T^{cons} against the experimental S_w , the linear regression coefficient found is $0.053 \pm 0.002^\circ\text{C}/(\text{g.kg}^{-1})$, close to the theoretical linear liquidus coefficient $\mu=0.0598^\circ\text{C}/(\text{g.kg}^{-1})$ for NaCl ice (see Fig. 6a).

Physically speaking, the strong control of the equilibrium temperature by the water salinity confirms that the largest energetic buffer in the system is the release (uptake) of latent heat by internal freezing (melting) – in direct association with S_w – whereas changing T_s or T_w requires only a small amount of heat. As a result, T^{cons} and T^{fr} are close (as long as the Stefan number is small and snow density is $< 600 \text{ kg/m}^3$ (see Fig. 3). In the enthalpy-temperature diagram (Fig. 2), the slope of E_i is nearly vertical close to freezing, which induces that $T_i \approx T^{fr}$. There are two additional consequences to keep in mind. First, the temperature of the newly formed snow ice can be lower than that of the pre-existing saltwater and snow (Table S1). Second, the T_w value above which the sensible heat stored in saltwater is large enough to melt all snow is very high ($> 40^\circ\text{C}$). This is why experiments with water at room temperature were possible and performed.

As expected, the temperature of the forming sea ice increases with T_w and T_s . However, because the Stefan number is small, these dependencies are small (see Fig. 6b-c), as predicted by the fully-conserving approach (eq. 3): T^{cons} changes by less than 0.05°C per degree of change in T_w or T_s .

If $\rho_s > 600 \text{ kg/m}^3$, the fully-conserving approach predicts a significant impact

of the snow and saltwater temperature on T_i , in contrast with the freezing point approach (Fig. 3). Density values larger than 582 kg/m^3 were not tested, however, and a minor influence of density on experimental results is indeed observed.

4.2. Brine fraction, cohesion and ice crystals flotation

With the linear liquidus assumption, brine fraction is given by $\phi_l = -\mu S_i/T_i$ (Ono, 1967). Combining the first-order temperature solution (eq. 4) and salt conservation (eq. 2a), one gets

$$\phi_l \approx \phi_a \quad (5)$$

as suggested in Section 2 for small Stefan number values.

The full model solution for brine fraction (color contours in Fig. 3) uses the computed value of S_i (eq. 2a) and T_i (eq. 3) and does not markedly differ from ϕ_a : brine fraction is practically determined by snow density alone and differences from the air fraction in the pre-existing snow are very small (< 0.05 , Fig. 3c).

Brine fraction was not measured during our experiments, but can be diagnosed from $-\mu S_i/T_i$. Changes in the cohesion of the experimental snow ice were observed depending on brine fraction. Below $\phi_l = 50\%$, the synthetic sea ice was wet and permeable but consolidated. In the range $50\% < \phi_l < 60\%$, the ice pieces became mobile and could easily be stirred, but cohesion was strong enough to resist buoyancy (cohesive slush). Above $\phi_l = 60\%$, the slush mixture had no more cohesion (loose slush) and ice crystals started to float (as shown by pictures in Fig. 7). Flotation implies the violation of **H2**: the system stratifies and is no more homogeneous. Indeed, experimental runs with $\phi_l > 60\%$ give temperatures outside model predictions.

5. Natural sea ice observations from the SIMBA experiment

To see how the snow-ice salinities and temperatures obtained from the enthalpy conservation calculations compare with what is observed in a natural context, we analyze ice temperature and salinity data from ice core sections in a floe that underwent occasional flooding during the SIMBA (Sea Ice Mass BALance of the Antarctic) research program, which took place in the Bellingshausen Sea from September 25 to October 24, 2007 (Lewis et al., 2011). The ice-temperature profile was measured in drill holes immediately after core extraction, texture was retrieved from thin sections, whereas salinity and oxygen isotope data were obtained from melted 5 cm-thick core sections (see Lewis et al., 2011, for more details on sampling and methods). 250 ice core sections from 13 cores taken at *Inbound*, *Brussels* and *Liège* sites were analyzed.

A sample was classified as snow ice if its texture was granular and its $\delta^{18}O$ was $< -2\text{‰}$, which corresponds to 20% of ice with meteoric origin (Jeffries et al., 1997). Core sections were classified as *snow ice* (19 samples), *granular ice* (144), *columnar ice* (87). All identified snow-ice samples lie in the upper third of the ice. A slush sample is also included in the analysis (Lewis et al., 2011). The characteristics of this sample are similar to those reported by other investigators in the Weddell Sea (Lytle and Ackley, 1996) and in the East Antarctic sector (Massom et al., 1998).

Each sample was represented in a T-S diagram (Fig. 8), with a different symbol for each ice type. Only the slush sample (triangle) has salinity and temperature that are consistent with theoretical predictions using the fully-conserving approach (dotted red line and pink and blue bands, respectively). The snow-ice samples (filled dots) have lower salinities and generally colder temperatures than predicted. This is because the closed system assumption does not hold very long in reality: newly formed slush and snow ice exchange heat and salt with their surroundings. As some

of the ice cores were taken 1-2 days after flooding, rapid heat and salt losses affect T and S and the description presented in Section 2 holds over a few hours at most.

Snow-ice samples are all significantly less saline than predictions from the energy-conserving approach (Schmidt et al., 2004). Such a systematic bias supports rapid and strong desalination, in agreement with the one-dimensional simulations of Maksym and Jeffries (2000, 2001) and Saenz and Arrigo (2012). Yet snow-ice samples are more saline (8.9 ± 2.6 g/kg) than other upper ice samples (5.6 ± 2.0 g/kg) and deeper ice samples (3.8 ± 1.2 g/kg). Finally, whether the flooding water is brine or seawater could have a specific footprint on temperature, but the SIMBA ice coring observations cannot be used to detect it: samples were collected too long after flooding, and the moment of flooding can hardly be identified.

6. Discussion and outlook

The simple energetic arguments and laboratory experiments presented here show that the temperature of slush or snow ice immediately after formation is very close to the freezing point of the flooding saltwater, and hence is primarily determined by the flooding saltwater salinity. Other factors, i.e. snow temperature, saltwater temperature and snow density have much smaller effects. Such physics derive from the large effect of the latent heat released (absorbed) by internal freezing (melting). The SIMBA temperature and salinity observations from ice cores (Bellingshausen Sea, spring 2007) suggest that the initial temperature and salinity of newly formed snow ice and slush hold for up to a few hours only, after which rapid heat exchanges and desalination processes destroy these initial signatures.

The description of slush and snow-ice formation used in most sea-ice models (e.g., Hunke et al., 2015; Vancoppenolle et al., 2009), based on the formalism of Schmidt et al. (2004), is appropriate to represent the energetic exchanges during

328 flooding events. The agreement found here between this formulation and laboratory
 329 experiments, within $< 0.1^{\circ}\text{C}$ on average, strengthens the confidence in the thermody-
 330 namic basis of sea-ice models. The water temperature limit for slush survival in an
 331 isolated system is extremely high ($> 40^{\circ}\text{C}$), hence the Schmidt et al. (2004) formula-
 332 tion can be used for virtually all situations encountered on this planet. Finally, note
 333 that the isolated system hypothesis, the most doubtable of all, is relieved in sea-ice
 334 models after the computation of slush and snow-ice initial properties: exchanges of
 335 salt and heat with the remainder of the ice are computed in a separate step. The
 336 largest remaining uncertainty is associated with the salinity of the flooding saltwa-
 337 ter. Most large-scale sea-ice models assume that seawater floods the snow. Yet the
 338 new snow-ice temperature could be significantly lower if models assumed that brine,
 339 much more saline than seawater, floods the snow, instead of seawater, with potential
 340 impacts on basal ice growth.

341 Laboratory experiments indicate flotation of ice crystals for brine fractions above
 342 60%, which corresponds to snow densities below 350 kg/m^3 . Such densities were
 343 rarely encountered in our experiments, but are frequent in nature (Massom et al.,
 344 2001), hence liquid water could be found near the snow-ice interface if enough slush
 345 is formed at a time, e.g. after a strong snow storm. Since our experiments were
 346 conducted in an idealized environment, it is hard to predict how these liquid layers
 347 would evolve in nature based on our experiments. Yet the finding of floating ice
 348 crystals above liquid water could relate to the reports of very wet conditions near
 349 the snow base (Lewis et al., 2011; Lytle and Ackley, 1996) and relate to what has
 350 been described as "gap layers" (Ackley et al., 1979; Haas et al., 2001) - liquid layers
 351 right below the ice-snow interface. Ice crystal flotation effects are not represented in
 352 sea-ice models, but we do not envision large impacts on simulated ice thickness.

353 The Schmidt et al. (2004) conservation equations suggest that the snow and salt-

water temperatures become influential for snow density above 600 kg/m^3 . Snow would rarely be so dense in nature, but using such large values could describe the flooding of denser ice forms, such as sea ice itself. In this regime, the impact of the sensible heat contained in the pre-existing ice becomes dominant and the resulting ice temperature is much closer to the pre-existing ice temperature.

The fully-conserving approach of Schmidt et al. (2004) as presented here may also somewhat apply to retrieve the temperature of ridged ice. Ridges are also mixtures of ice and saltwater, but with large chunks of ice instead of microscopic crystals. Within ridges, however, the time scale to equilibrium would be a few days (Høyland, 2002), being governed by heat diffusion in the ice blocks and convection in the liquid voids, rather than by salt diffusion.

Several uncertainties remain regarding the representation of Antarctic sea-ice thermodynamics in large-scale models. Whether the latter need to capture all the halo-thermodynamic processes specific to the Antarctic sea-ice zone (Kawamura et al., 1997; Lewis et al., 2011; Lytle and Ackley, 1996) remains unclear. How brine and seawater sources contribute to flooding is not well understood, neither how the salt losses and heat exchanges shape the evolution of slush and snow ice after formation, as already pointed out (Maksym and Jeffries, 2000; Saenz and Arrigo, 2012). Our understanding could improve from natural and experimental sea-ice studies, in particular through the use of non-destructive and high frequency temperature and salinity measurements, as proposed by Notz (2005a), rather than from ice coring.

Appendix A. Computation of slush and snow-ice properties in sea-ice models

The initial state of the system is characterized by a snow mass m_s – with temperature T_s , zero salinity, and density ρ_s – homogeneously flooded by an appropriate mass of saltwater m_w with temperature T_w and salinity S_w (that of seawater or brine). Snow and saltwater are then mixed homogeneously. The final state is a mass of sea ice m_i with temperature T_i and salinity S_i .

As described in Section 2, we assume an isolated system (**H1**), evolving towards thermodynamic equilibrium (**H2**), and that the flooding water entirely fills the air initially present in the snow (**H3**). We further assume that the densities of snow (ρ_s), sea ice (ρ_i) and the latent heat of fusion of pure ice (L) as well as the pure ice and saltwater heat capacities (c_0 , c_w) are independent of T and S (see Tab. 1). We also assume that the sea-ice liquidus is linear: $T = -\mu S_{br}$, where S_{br} is brine salinity and μ corresponds to either sea ice or NaCl ice (see Tab. 1). This is valid as long as energetic exchanges are considered, but not for a precise computation of brine salinity (Notz, 2005b).

Following **H1** and **H2**, the water, salt and energy conservation laws of the system read (in order):

$$m_i = m_s + m_w, \quad (\text{A.1a})$$

$$m_i S_i = 0 + m_w S_w, \quad (\text{A.1b})$$

$$m_i E_i = m_s E_s + m_w E_w, \quad (\text{A.1c})$$

where the specific enthalpies (J/kg) of snow ice, snow and saltwater are respectively

(Schmidt et al., 2004):

$$E_s(T_s) = c_0 T_s - L, \quad (\text{A.2a})$$

$$E_w(T_w) = c_w T_w, \quad (\text{A.2b})$$

$$E_i(T_i, S_i) = c_0 (T_i + \mu S_i) - L \left(1 + \frac{\mu S_i}{T_i} \right) - c_w \mu S_i. \quad (\text{A.2c})$$

The expression for E_i is based on the linear liquidus hypothesis. Using **H3**, the system of equations (A.1) can be rewritten as:

$$m_w = (\rho_i - \rho_s) V, \quad (\text{A.3a})$$

$$S_i = \phi_a S_w, \quad (\text{A.3b})$$

$$E_i(T_i, S_i) = \phi_i E_s(T_s) + \phi_a E_w(T_w), \quad (\text{A.3c})$$

where $\phi_i = \rho_s / \rho_i$ and $\phi_a = (\rho_i - \rho_s) / \rho_i$ are the ice and air fractions in the pre-existing snow, respectively. The system (A.3) thermodynamically describes new slush and snow-ice formation and gives m_w , S_i and T_i , assuming that T_w , S_w and T_s are known. The first two equations are trivial. For the temperature equation, we replace the specific enthalpies in (A.3c) by their expressions from (A.2), then multiply by T_i and replace S_i by its expression (A.3b), giving:

$$0 = c_0 T_i^2 - A(T_w, S_w, T_s) \cdot T_i - \phi_a L \mu S_w, \quad (\text{A.4a})$$

$$A(T_w, S_w, T_s) = \phi_i c_0 T_s + \phi_a \left[L + c_w T_w + (c_w - c_0) \mu S_w \right]. \quad (\text{A.4b})$$

Equation (A.4a) is quadratic in T_i , with a unique physically acceptable solution.

Appendix B. Material and methods

The main series of laboratory experiments was conducted at the *Laboratoire d'Océanographie et du Climat, Paris*, in June 2014. The micro-structure of grated

ice and of synthetic snow ice was examined in a separate series of experiments in a cold room at the *Laboratoire de Glaciologie, Université Libre de Bruxelles, Belgium* (see Fig. 4) in January 2015.

Grated ice was obtained by grating tap water ice cubes with a professional cheese grater (Santos no. 2), with two different blades to get different densities (see Fig. 4a). Grated ice was used as an analog for snow, as it is more easily obtained, at least in Paris where the experiments took place. Grated ice density is hard to control accurately, but we obtain a range from 462-582 kg/m³ and use snow from condensation in a freezer with $\rho_s = 332\text{-}438$ kg/m³. Like for snow, grated ice includes ice and air, hence at macro-scales, its action on heat diffusion is similar. The grated ice grains are typically less than ~ 3 mm-long, only slightly larger than natural snow grains (1-2 mm Massom et al., 2001), and much smaller than the scale of the experiment (about 2L), which is important to ensure that **H2** is verified. The grains are also more acute (Fig. 4c) than for natural snow (Fig. 4d), but this should not affect the heat diffusion. All these arguments give enough support to the use of grated ice for our purposes.

The saltwater was obtained by diluting NaCl caps in tap water. The salinity of this water and that of the melted synthetic snow ice were retrieved from high-precision density measurements, using a centigram precise balance and a high precision flask for volume measurement. Density (ρ) was converted into salinity using the TEOS-10 software (IOC et al., 2010). The error in salinity was calculated by comparing the maximal and minimal values obtained by using $\rho \pm \Delta\rho$, where $\Delta\rho$ is the measurement uncertainty on density. The resulting typical error in salinity was ~ 1 g/kg.

Grated ice density was derived by weighing ~ 2 L of grated ice and measuring its volume with a long graduated cylinder. The uncertainty in volume estimates is on

the order of $\Delta V \approx 50$ mL due to (i) changes in grated ice density and loss of ice during transfer from the cylinder to the cryogenic container and (ii) irregularities at the grated ice surface. This leads to an error in $\Delta\rho_s$ of ≈ 30 kg/m³, i.e. a few percent of the absolute value.

The saltwater temperature ranged from -1.2°C to 23.7°C, being measured with a Testo 720 digital thermometer ($\Delta T = \pm 0.1^\circ\text{C}$). The temperature in the cryogenic container – before and after pouring the saltwater – was measured with a homemade thermistor chain ($\Delta T = \pm 0.02^\circ\text{C}$, one sensor every 6 cm, sampling every 4 seconds). Both temperature sensors were calibrated using a Sea Bird temperature logger ($\Delta T = \pm 10^{-3}^\circ\text{C}$) as a standard measure.

Acknowledgments

European Union funding through BISICLO (FP7 Career Integration Grant 321938) is gratefully acknowledged. For SIMBA data, please contact Jean-Louis Tison (jtison@ulb.ac.be). Thanks as well to François Fripiat for lending us his precious professional cheese grater. Anonymous reviewers made relevant, significant and highly appreciated suggestions that really helped in improving this manuscript.

References

- Ackley, S.F., Buck, K., S.Taguchi, 1979. Standing crop of algae in the sea ice of the Weddell Sea region. *Deep-Sea Research, Part A* 26, 269–281.
- Bitz, C.M., Lipscomb, W.H., 1999. An energy-conserving thermodynamic model of sea ice. *Journal of Geophysical Research* 104, 15,669–15,677.

- 469 Bromwich, D.H., Guo, Z., Bai, L., Chen, Q.S., 2004. Modeled Antarctic precipi-
470 tation. part i: Spatial and temporal variability. *Journal of Climate* 17, 427–447.
471 doi:10.1175/1520-0442(2004)017<0427:MAPPIS>2.0.CO;2.
- 472 Crocker, G.B., Wadhams, P., 1989. Modelling Antarctic fast-ice growth. *Journal of*
473 *Glaciology* 35, 3–8. doi:10.3189/002214389793701590.
- 474 Eicken, H., Lange, M.A., Wadhams, P., 1994. Characteristics and distribution pat-
475 terns of snow and meteoric ice in the Weddell Sea and their contribution to the
476 mass balance of sea ice. *Annales Geophysicae* 12, 80–93.
- 477 Fichefet, T., Morales Maqueda, M.A., 1997. Sensitivity of a global sea ice model
478 to the treatment of ice thermodynamics and dynamics. *Journal of Geophysical*
479 *Research* 102, 12,609–12,646.
- 480 Golden, K.M., Ackley, S.F., Lytle, V.I., 1998. The percolation phase transition in
481 sea ice. *Science* 282, 2238–2241. doi:10.1126/science.282.5397.2238.
- 482 Haas, C., Thomas, D.N., Bareiss, J., 2001. Surface properties and processes
483 of perennial Antarctic sea ice in summer. *Journal of Glaciology* 47, 613–625.
484 doi:10.3189/172756501781831864.
- 485 Høyland, K.V., 2002. Consolidation of first-year sea ice ridges. *Journal of Geophysical*
486 *Research* 107, 3062. doi:10.1029/2000JC000526.
- 487 Høyland, K.V., 2009. Ice thickness, growth and salinity in Van
488 Mijenfjorden, Svalbard, Norway. *Polar Research* 28, 339–352.
489 doi:10.1111/j.1751-8369.2009.00133.x.

- 490 Hunke, E.C., Lipscomba, W.H., Turner, A.K., Jeffery, N., Elliott, S., 2015. CICE:
491 the Los Alamos sea ice model documentation and software user's manual version
492 5.1. Technical Report, Los Alamos National Laboratory, Los Alamos, New Mexico.
- 493 IOC, SCOR, IAPSO, 2010. The international thermodynamic equation of seawater -
494 2010: Calculation and use of thermodynamic properties. Intergovernmental
495 Oceanographic Commission, Manuals and Guides 56, UNESCO.
- 496 Jeffries, M., Worby, A., Morris, K., Weeks, W.F., 1997. Seasonal variations in the
497 properties and structural composition of sea ice and snow cover in the Belling-
498 shausen and Amundsen Seas, Antarctica. *Journal of Glaciology* 43, 138–151.
- 499 Jeffries, M.O., Krouse, H.R., Hurst-Cushing, B., Maksym, T., 2001. Snow-ice ac-
500 cretion and snow-cover depletion on Antarctic first-year sea-ice floes. *Annals of*
501 *Glaciology* 33, 51–60. doi:10.3189/172756401781818266.
- 502 Kawamura, T., Ohshima, K.I., Takizawa, T., , Ushio, S., 1997. Physical, structural
503 and isotopic characteristics and growth processes of fast sea ice in Lützow-Holm
504 Bay, Antarctica. *Journal of Geophysical Research* 102, 3345–3355.
- 505 Leppäranta, M., 1983. A growth model for black ice, snow ice and snow thickness in
506 subarctic basins. *Nordic Hydrology* 14, 59–70. doi:10.2166/nh.1983.006.
- 507 Leppäranta, M., Lensu, M., Witch, P.K.B., 1995. The life story of a
508 first-year sea ice ridge. *Old Regions Science and Technology* 23, 279–290.
509 doi:10.1016/0165-232X(94)00019-T.
- 510 Lewis, M.J., Tison, J.L., Weissling, B., Delille, B., Ackley, S., Brabant, F., Xie, H.,
511 2011. Sea ice and snow cover characteristics during the winter-spring transition in

- the Bellingshausen Sea: An overview of SIMBA 2007. *Deep Sea Research (II)* 58,
1019–1038. doi:10.1016/j.dsr2.2010.10.027.
- Lytle, V., Ackley, S., 1996. Heat flux through sea ice in the Western Weddell Sea:
Convective and conductive transfer processes. *Journal of Geophysical Research*
101, 8853–8868.
- Maksym, T., Jeffries, M., 2001. Phase and compositional evolution of the flooded
layer during snow-ice formation on Antarctic sea ice. *Annals of Glaciology* 33,
37–44.
- Maksym, T., Jeffries, M.O., 2000. A one-dimensional percolation model of flooding
and snow ice formation on Antarctic sea ice. *Journal of Geophysical Research* 105,
26,313–26,331.
- Maksym, T., Markus, T., 2008. Antarctic sea ice thickness and snow-to-ice conver-
sion from atmospheric reanalysis and passive microwave snow depth. *Journal of*
Geophysical Research 113. doi:10.1029/2006JC004085.
- Massom, R.A., Eicken, H., Haas, C., Jeffries, M.O., Drinkwater, M.R., Sturm, M.,
Worby, A.P., Wu, X., Lytle, V.I., Ushio, S., Morris, K., Reid, P.A., Warren, S.G.,
Allison, I., 2001. Snow on Antarctic sea ice. *Review of Geophysics* 39, 413–445.
- Massom, R.A., Lytle, V., Worby, A.P., Allison, I., 1998. Winter snow cover variability
on East Antarctic sea ice. *Journal of Geophysical Research* 103, 24,837–24,855.
- Maykut, G.A., Untersteiner, N., 1971. Some results from a time-dependent thermo-
dynamic model of sea ice. *Journal of Geophysical Research* 76, 1550–1575.

- 533 Notz, D., 2005a. A non-destructive method for measuring the salinity and
 534 solid fraction of growing sea ice in situ. *Journal of Glaciology* 51, 159–166.
 535 doi:10.3189/172756505781829548.
- 536 Notz, D., 2005b. Thermodynamic and fluid-dynamical processes in sea ice. Ph.D.
 537 thesis, University of Cambridge .
- 538 Ono, N., 1967. Physics of snow and ice, chap. Specific heat and heat of fusion of sea
 539 ice. Institute of Low Temperature Science, Hokkaido, Japan , 599–610.
- 540 Saenz, B.T., Arrigo, K.R., 2012. Simulation of a sea ice ecosystem using a hybrid
 541 model for slush layer desalination. *Journal of Geophysical Research* 117, 1–20.
 542 doi:10.1029/2011JC007544.
- 543 Schmidt, G., Bitz, C.M., Mikolajewicz, U., Tremblay, L.B., 2004. Ice-
 544 ocean boundary conditions for coupled models. *Ocean Modelling* 7, 59–74.
 545 doi:10.1016/S1463-5003(03)00030-1.
- 546 Squire, V.A., 2007. Of ocean waves and sea-ice revisited. *Cold Regions Science and*
 547 *Technology* 49, 110–133. doi:10.1016/j.coldregions.2007.04.007.
- 548 Tin, T., Jeffries, M., 2003. Morphology of deformed first-year sea ice features
 549 in the Southern Ocean. *Cold Regions Science and Technology* 36, 141–163.
 550 doi:10.1016/S0165-232X(03)00008-9.
- 551 Vancoppenolle, M., Fichefet, T., Goosse, H., Bouillon, S., Madec, G., Morales
 552 Maqueda, M.A., 2009. Simulating the mass balance and salinity of Arctic and
 553 Antarctic sea ice. 1. Model description and validation. *Ocean Modelling* 27, 33–53.
 554 doi:10.1016/j.ocemod.2008.10.005.

- 555 Vancoppenolle, M., Goosse, H., de Montety, A., Fichefet, T., Tremblay, B., Ti-
556 son, J.L., 2010. Modeling brine and nutrient dynamics in Antarctic sea ice:
557 the case of dissolved silica. *Journal of Geophysical Research* 115, C02005.
558 doi:10.1029/2009JC005369.
- 559 Williams, G., Maksym, T., Wilkinson, J., Kunz, C., Murphy, C., Kimball, P., Singh,
560 H., 2014. Thick and deformed Antarctic sea ice mapped with autonomous under-
561 water vehicles. *Nature Geoscience* 8, 61–67. doi:10.1038/ngeo2299.
- 562 Worby, A., Massom, R., Allison, I., Lytle, V.I., Heil, P., 1998. Antarctic sea ice:
563 Physical processes, interactions and variability. *Antarctic Research Series*, chap.
564 East Antarctic sea ice: A review of its structure, properties and drift, AGU 74,
565 89–122.
- 566 Worby, A.P., Geiger, C.A., Paget, M.J., Woert, M.L.V., Ackley, S.F., DeLiberty,
567 T.L., 2008. The thickness distribution of Antarctic sea ice. *Journal of Geophysical*
568 *Research* 113, C05S92. doi:.1029/2007JC004254,.

Table 1: Physical constants.

<i>Symbol</i>	<i>Definition</i>	<i>Value</i>	<i>Units</i>	<i>Reference</i>
c_0	Heat capacity (pure ice)	2110	J/(kg.K)	Bitz and Lipscomb (1999)
c_w	Heat capacity (saltwater)	3992	J/(kg.K)	IOC et al. (2010)
L	Latent heat of fusion (pure ice)	334×10^3	J/kg	Bitz and Lipscomb (1999)
μ_{NaCl}	Linear dependence of liquidus (NaCl ice)	0.0598	$^{\circ}\text{C}/(\text{g}/\text{kg})$	Notz (2005b)
μ_{si}	Linear dependence of liquidus (sea ice)	0.054	$^{\circ}\text{C}/(\text{g}/\text{kg})$	Notz (2005b)
ρ_s	Density (snow)	100-600	kg/m^3	Massom et al. (2001)
ρ_i	Density (sea ice)	950	kg/m^3	This study

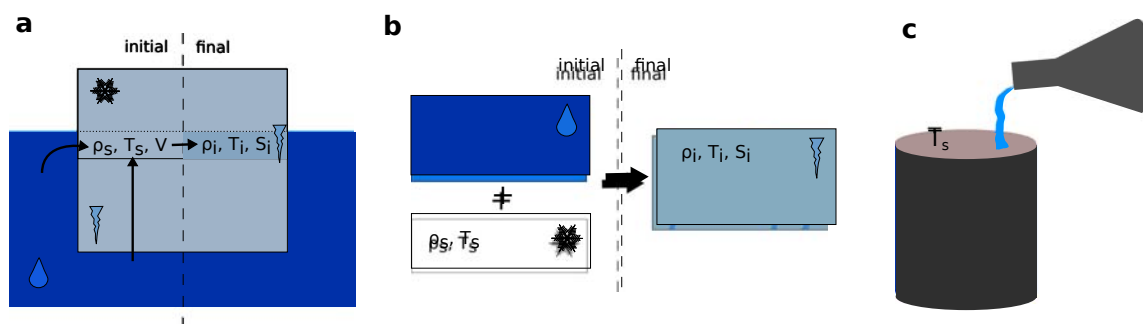


Figure 1: Schematics of a flooding event (a) in the field, (b) as viewed in sea-ice models, and (c) in the laboratory experiments described in this paper. ρ represents density, m mass, V volume, T temperature and S salinity. The subscript w stands for water, i for ice and s for snow.

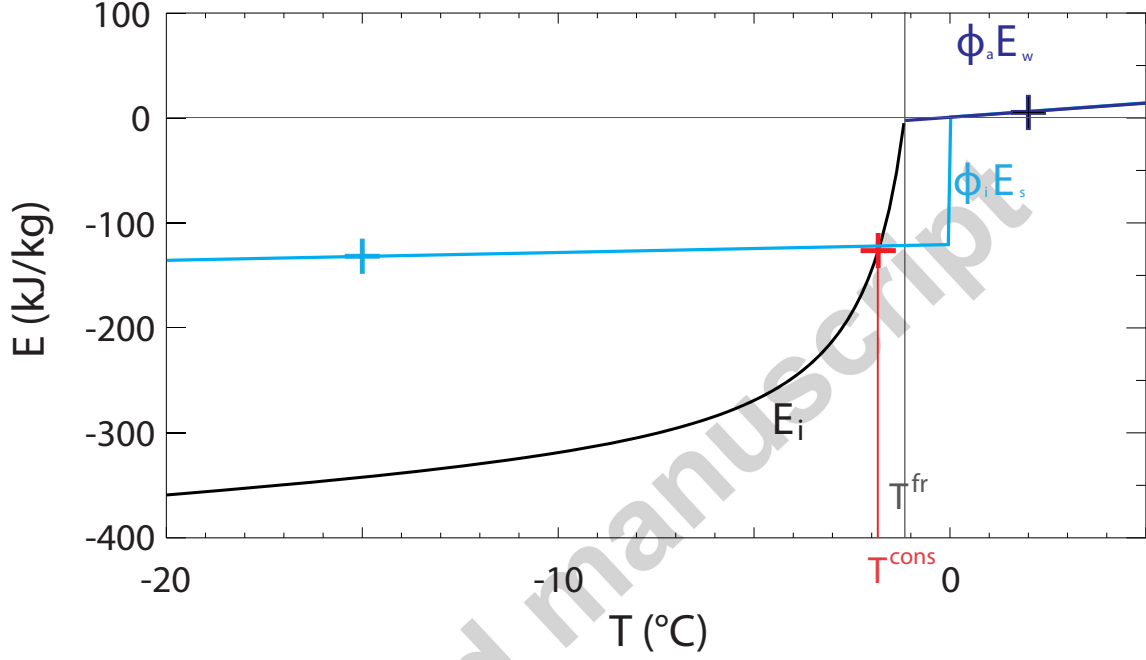


Figure 2: Enthalpy-temperature diagram for snow ice formation as represented in the fully-conserving approach (Schmidt et al., 2004, eq. 2b), showing the snow-ice enthalpy (E_i , black line), as well as the weighted contributions of snow enthalpy ($\phi_i E_s$, light blue line) and saltwater enthalpy ($\phi_a E_w$, deep blue line). A sample experiment is depicted (crosses) where snow with $T_s = -15^\circ\text{C}$ (light blue) is flooded by saltwater with $T_w = 2^\circ\text{C}$ (deep blue). The resulting snow-ice enthalpy is $\phi_i E_s + \phi_a E_w$ (red). The resulting snow-ice temperature T^{cons} (eq. 3) can be graphically retrieved as the abscissa of the red cross. The freezing point of flooding saltwater (T^{fr} , eq. 1) is also indicated. The diagram was constructed using $\rho_s = 330 \text{ kg/m}^3$ and $S_w = 34 \text{ g/kg}$, giving, $\phi_i = 0.35$, $\phi_a = 0.65$ and $S_i = 21.8 \text{ g/kg}$.

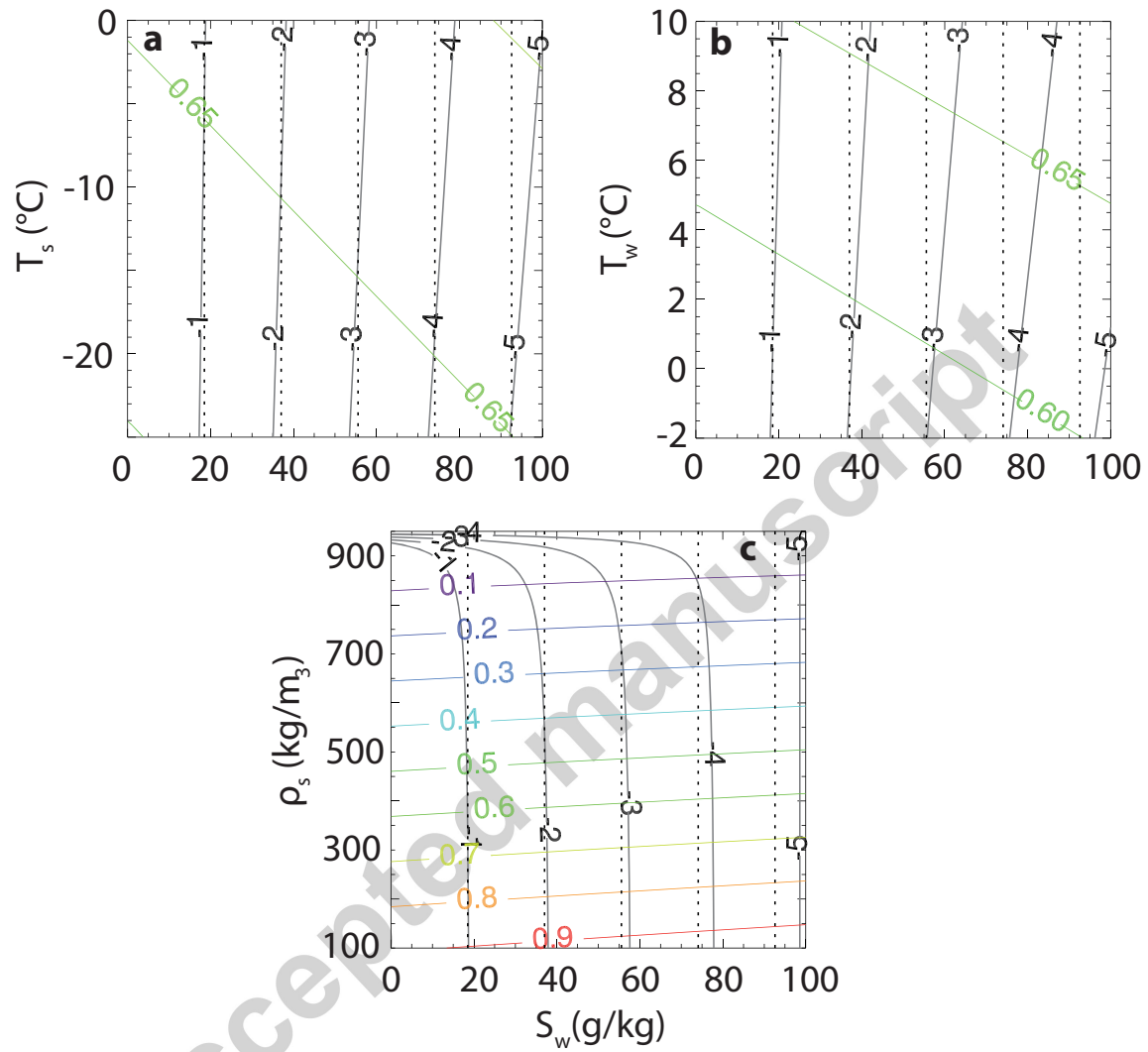


Figure 3: Snow-ice temperature (black) and brine fraction (color) isolines for various input parameter combinations, retrieved from the fully-conserving approach (eq. 2b, Schmidt et al., 2004, solid lines). Black dashed lines represent the freezing point of flooding saltwater (eq. 1). In panel (a) $\rho_s = 330$ kg/m³ and $T_w = 0^\circ\text{C}$; in (b) $\rho_s = 330$ kg/m³ and $T_s = -5^\circ\text{C}$ and in (c) $T_w = 0^\circ\text{C}$ and $T_s = -5^\circ\text{C}$. Those values are assumed typical of natural conditions.

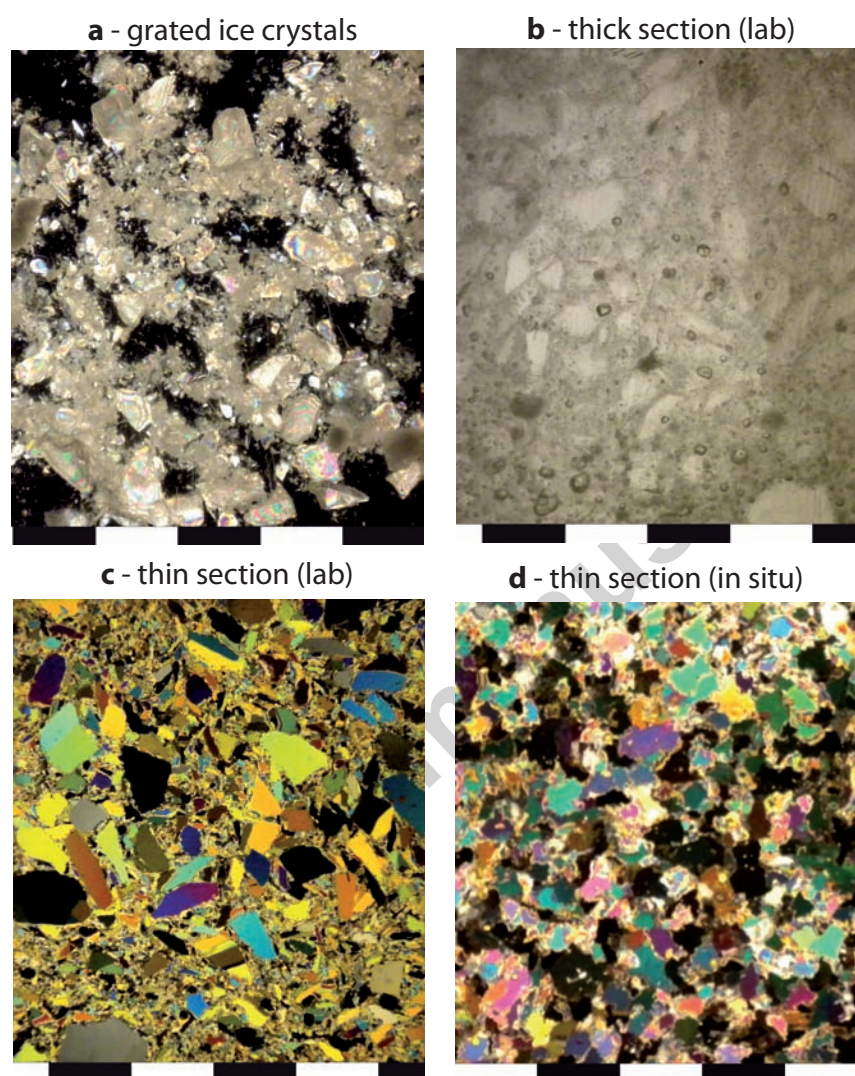


Figure 4: Cold room textural analysis of (a) unpacked grated ice crystals; (b) thick (0.5 cm) and (c) thin sections (0.8 mm) from synthetic snow ice (lab); (d) thin section (0.8 mm) from natural sea ice identified as snow ice from the SIMBA campaign, sampled at *Liège* site, station 2, Oct 8, 2007 (Lewis et al., 2011). The rules indicate 1-cm spacings.

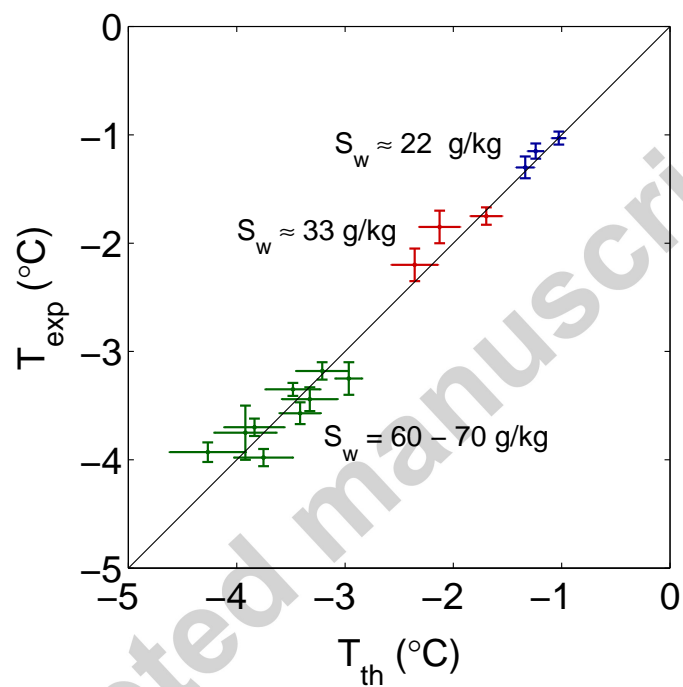


Figure 5: Snow-ice temperature: experimental versus retrieved (fully-conserving approach, Schmidt et al., 2004, eq. 3), for different sets of input physical parameters, and grouped for different saltwater salinities. The crosses represent the experimental and theoretical uncertainty range.

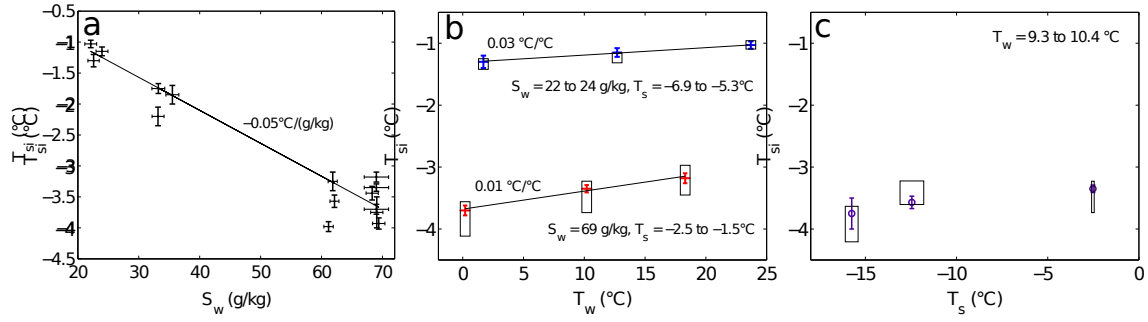


Figure 6: Observed snow-ice temperature versus (a) water salinity, (b) water temperature and (c) snow temperature in the laboratory experiments. The squares are the retrieved values (fully-conserving approach, Schmidt et al., 2004, eq. 3), including uncertainty. For each experiment we attempted to change a single parameter at a time, which was not easy to achieve and explains most of the scatter.

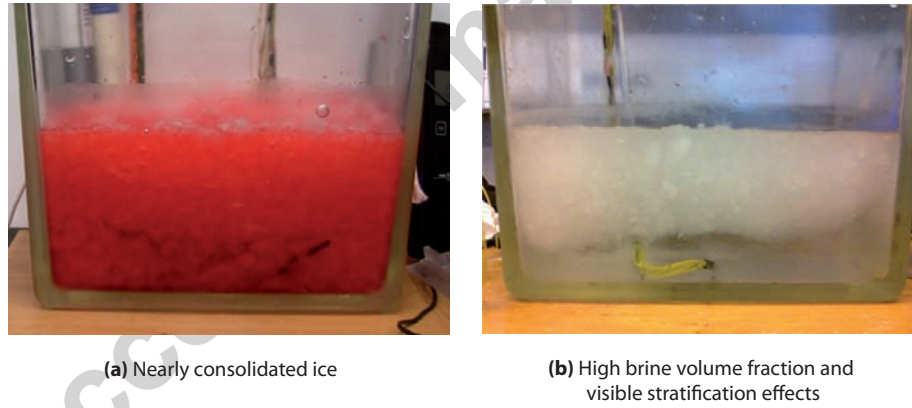


Figure 7: Impact of brine fraction on ice flotation, for two sample experiments performed in a glass container rather than in the cryogenic container for visualization purposes. In (a) the brine fraction is small enough to prevent flotation, hence the system reaches thermodynamic equilibrium. In (b) the brine fraction is $\approx 80\%$, the ice matrix is not solid enough, stratification occurs and **H2** is not verified. The ice on the left picture is red because of a dye.

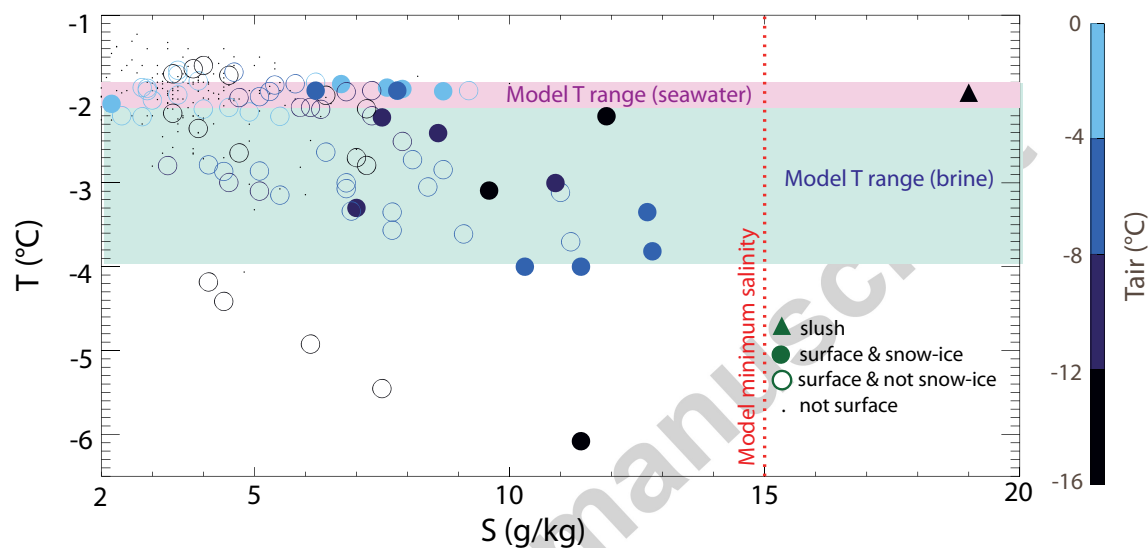


Figure 8: Sea-ice temperature versus salinity from the SIMBA samples: slush (\triangle); deep ice-core sections ($z \geq h_i/3$, \cdot) and surface ice-core sections ($z < h_i/3$, \circ). Filled symbols indicate samples classified as snow ice ($\delta^{18}O < -2\text{‰}$ and granular texture). The retrieved temperature and salinity ranges (fully-conserving approach, Schmidt et al., 2004, eq. 2b and 3) are also depicted. The pink and blue bands refer to the predicted temperature range (pink if the flooding water is seawater, blue if this is brine). The red vertical dotted line is the lowest expected snow-ice salinity (using $\rho_s = 500 \text{ kg/m}^3$ and $S_w = 34 \text{ g/kg}$).

Table S1: Summary of experimental results. $T_i^{fr} = -\mu S_w$ (Eq. 1), and the T_i^{cons} is retrieved from the fully-conserving approach (Schmidt et al., 2004, Eq. 3). Brine volume is computed from $\phi_l = -\mu S_i/T_i$, using measured S_i and T_i . The last seven experiments have a brine fraction (ϕ_l) exceeding our model range of applicability (> 60 kg/m³), which is why the model experiment discrepancy is larger.

T_w ($\pm 0.1^\circ\text{C}$)	T_s ($^\circ\text{C}$)	ρ_s (kg/m ³)	S_w (g/kg)	T_i^{exp} ($^\circ\text{C}$)	T_i^{fr} ($\pm 0.1^\circ\text{C}$)	T_i^{cons} ($^\circ\text{C}$)	ϕ_l (%)
0.2	-1.5 ± 0.1	561 ± 11	69 ± 2	-3.70 ± 0.08	-4.1	-3.8 ± 0.3	46 ± 3
10.2	-2.52 ± 0.07	561 ± 11	69 ± 2	-3.4 ± 0.06	-4.1	-3.5 ± 0.2	51 ± 4
18.3	-2.26 ± 0.08	567 ± 11	69 ± 2	-3.2 ± 0.08	-4.1	-3.2 ± 0.2	52 ± 4
3.0	-15.3 ± 0.3	578 ± 12	69 ± 1	-3.93 ± 0.09	-4.1	-4.2 ± 0.5	34 ± 3
10.4	-15.8 ± 0.4	578 ± 12	69 ± 1	-3.8 ± 0.3	-4.1	-3.9 ± 0.4	36 ± 4
17.2	-6.4 ± 0.8	578 ± 12	68 ± 1	-3.4 ± 0.1	-4.1	-3.3 ± 0.4	40 ± 3
6.1	-26.3 ± 0.6	582 ± 12	33 ± 1	-2.20 ± 0.15	-2.0	-2.3 ± 0.4	45 ± 6
11.9	-18.3 ± 0.6	582 ± 12	35 ± 1	-1.85 ± 0.15	-2.1	-2.1 ± 0.4	38 ± 7
23.0	-14.5 ± 0.4	582 ± 12	33 ± 1	-1.75 ± 0.08	-2.0	-1.7 ± 0.3	36 ± 6
-1.2	-11.3 ± 0.8	500 ± 15	61.1 ± 0.8	-4.0 ± 0.8	-3.7	-3.7 ± 0.4	40 ± 2
9.3	-12.5 ± 0.7	515 ± 10	62.1 ± 0.8	-3.6 ± 0.1	-3.7	-3.4 ± 0.3	45 ± 2
20.8	-10.5 ± 0.4	494 ± 8	61.8 ± 0.8	-3.25 ± 0.15	-3.7	-3.0 ± 0.2	62 ± 3
1.0	-8.1 ± 0.9	549 ± 13	62 ± 1	-4.0 ± 0.1	-3.7	-3.6 ± 0.4	44 ± 3
10.4	-10 ± 1	540 ± 15	62 ± 1	-3.8 ± 0.2	-3.7	-3.3 ± 0.4	40 ± 3
21.0	-9.2 ± 0.4	549 ± 14	62 ± 1	-3.33 ± 0.06	-3.7	-3.0 ± 0.3	50 ± 4
3.7	-3.6 ± 0.4	484 ± 22	61.5 ± 0.8	-3.6 ± 0.2	-3.7	-3.4 ± 0.4	45 ± 2
11.7	-5.3 ± 0.5	489 ± 10	61.0 ± 0.8	-3.4 ± 0.2	-3.6	-3.1 ± 0.2	51 ± 3
18.6	-2.0 ± 0.2	462 ± 9	61.7 ± 0.8	-3.03 ± 0.09	-3.7	-2.9 ± 0.2	50 ± 2
23.7	-5.7 ± 0.3	400 ± 8	22 ± 1	-1.03 ± 0.06	-1.3	-1.0 ± 0.1	66 ± 11
12.7	-5.3 ± 0.4	396 ± 8	24 ± 1	-1.15 ± 0.07	-1.4	-1.2 ± 0.2	63 ± 10
1.7	-6.9 ± 0.3	402 ± 8	23 ± 1	-1.3 ± 0.1	-1.4	-1.4 ± 0.2	63 ± 9
2.3	-1.4 ± 0.2	332 ± 7	61.0 ± 0.8	-3.58 ± 0.07	-3.6	-3.4 ± 0.2	59 ± 3
10.2	-6.9 ± 0.3	344 ± 7	60.7 ± 0.8	-3.36 ± 0.07	-3.6	-3.1 ± 0.2	66 ± 3
20.5	-5.3 ± 0.3	370 ± 6	61.3 ± 0.8	-3.08 ± 0.08	-3.7	-2.9 ± 0.2	65 ± 4
9.0	-0.8 ± 0.6	438 ± 4	61.4 ± 0.8	-2.9 ± 0.2	-3.7	-3.1 ± 0.2	69 ± 4